Available online at www.sciencedirect.com

ScienceDirect

Physics Procedia 83 (2016) 1160 – 1169

Physics Procedia

9th International Conference on Photonic Technologies - LANE 2016

Evaluation and calibration of LCoS SLM for direct laser structuring with tailored intensity distributions

Johannes Strauß[a,b,*], Tom Häfner[a,b], Michael Dobler[a,b], Johannes Heberle[a,b], Michael Schmidt[a,b,c]

[a]*Institute of Photonic Technologies (LPT), Friedrich-Alexander-Universität Erlangen-Nürnberg, Konrad-Zuse-Straße 3-5, 91052 Erlangen, Germany*

[b]*Erlangen Graduate School in Advanced Optical Technologies (SAOT), Paul Gordan Straße 6, 91052 Erlangen, Germany*

[c]*Bayerisches Laserzentrum GmbH (blz), Konrad-Zuse-Straße 2-6, 91052 Erlangen, Germany*

Abstract

Tailored intensity distribution enables efficient microstructuring as the maximum pulse energy of an ultrashort-pulsed laser can be applied. Dynamic adaptation of the intensity profile can be realized by holographic laser beam shaping using phase-only liquid crystal on silicon (LCoS) displays as a spatial light modulator (SLM). To achieve the desired intensity profile at the focal plane an accurate phase retardation of the SLM's liquid crystals has to be guaranteed. In this publication we present the phase calibration of three LCoS SLM from different manufacturers. Each system is evaluated for direct laser structuring applications. As one of the tested SLM show a spatially nonlinear behavior, a compensation method proposed by *Engström et al.* in 2013 is applied. Finally, the necessity of this phase calibration is presented and discussed by applying a squared flat-top profile.

Peer-review under responsibility of the Bayerisches Laserzentrum GmbH

Keywords: laser; diffractive optics; holographic beam shaping; spatial light modulator

1. Introduction

Ultrashort-pulsed (USP) laser based processes are an opportunity to generate features in the micrometer range with high reproducibility due to non-thermal material removal. The excellent quality of such microstructures is based on the occurrence of minimal heat affected zones (HAZ) [Chichkov et al. (1996)]. Cold ablation provides advantages for many applications. By avoiding melt bumps further post-processing of topography sensitive textured surfaces in tribological systems such as forming tools is not required [Häfner et al. (2013)]. The unique dimensional

* Corresponding author. Tel.: +49-9131-85-23237 ; fax: +49-9131-85-23234 .
E-mail address: johannes.strauss@lpt.uni-erlangen.de

Peer-review under responsibility of the Bayerisches Laserzentrum GmbH
doi:10.1016/j.phpro.2016.08.122

accuracy of microstructured surfaces and minimal thermal load on surrounding material is important for electronic components such as solar cells, too. In solar cell processing, the selective ablation of thin layers e.g. molybdenum (P3 process step) requires tailored intensity distribution. Zones of the Gaussian beam profile above the ablation threshold induce USP specific cold ablation due to the removal of the heated material, but zones which are below the ablation threshold generate unwanted residual heat and this results in the generation of an HAZ [Gecys et al. (2011)]. These HAZ can be avoided by applying a top-hat shaped intensity distribution [Bischoff et al. (2015)]. The intensity distribution is even more important in ablation of temperature-sensitive diamond-like carbon (DLC) coatings. As these DLC coatings are advantageous in tribological applications due to their unique chemical and mechanical properties, unwanted heat input due to laser processing would result in partially graphitized zones [Donnet et al. (2008)]. The undesired change of material properties affect friction and can decrease tribological performance. Therefore, material and microstructure geometry dependent energy input is desirable in many applications to benefit from the advantages of USP laser processing. Furthermore, investigations on the acceleration of USP laser processes target higher productivity, which is important in industrial applications. For process parallelization under the constraint of high structure quality the pulse energy which is available by high performance USP laser sources has to be distributed on the substrate [Rung et al. (2014)]. Holographic beam shaping by a spatial light modulator (SLM) is an adequate approach to fulfill the requirements on USP processing regarding high quality and high efficiency.

The realization of an efficient beam shaping process requires a defined retardation of the spatial phase of the laser beam. As the exact phase retardation of each SLM represents manufacturer specific expertise, the spatial dependency of this function is measured in this paper. The measured variations are compensated to achieve a desired phase retardation. The effect of this calibration on the accuracy of microstructuring is discussed and the importance for the efficiency of beam shaping as well as in general micro material processing is shown. Thus, sufficient diffraction efficiency, which is necessary for efficient beam shaping with high pulse energy lasers, is targeted by the calibration of the SLM.

2. Methods

2.1. Experimental setup for phase response measurement

In our studies, SLMs from Hamamatsu, Holoeye and Boulder Nonlinear Systems (BNS) are examined for material processing. The phase response of each system is measured to enable the proper control of the phase retardation. For that purpose, the raw beam of a laser at 532 nm or 1064 nm is expanded with a pair of lenses (L1 and L2 in Fig. 1) to have a $1/e^2$ beam diameter corresponding to the diagonal length of the SLM. The laser beam is reflected at the SLM's active area at a minimum incident angle of 7°. Then the laser beam propagates through the lens L3 (Thorlabs, LA1461-C, f = 250 mm) which converts the phase modulated laser beam into the far-field intensity distribution. In the focal plane of the lens L3 a pinhole is mounted that allows only the first order of diffraction to pass. The transmitted laser power is recorded with a power meter (Coherent, PowerMax-USB UV/VIS Quantum Power Sensor).

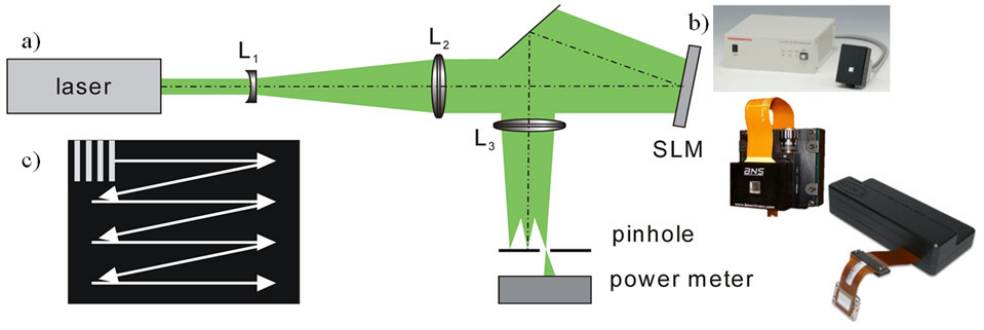

Fig. 1. (a) Setup to measure the phase function, (b) the three tested SLMs and (c) the strategy of measuring the phase function locally.

2.2. Determination of the phase function

The knowledge of the phase response acquired by the phase response measurement is important when a SLM is used for holographic laser beam shaping. It enables the calibration and linearization of the system [Engström et al. (2013)]. The phase function is evaluated by the acquisition of the laser power in the first order of diffraction depending on the control value (cv) when a binary grating is applied. The step height of the binary grating is successively incremented. The phase function is determined for 8 by 8 sections in order to take spatial differences of the LCoS into account. While the grating is displayed in one section only, the rest of the display remains at a constant bit level. This measurement is subsequently done for each section. The sequence of the spatially resolved phase measurement is shown in Fig. 1c). The measured laser power is normalized for all 64 data sets and the mean value and the standard deviation are calculated. The phase function is calculated from each normalized power function P(cv) according to eq. (1) and then the mean phase function is calculated. The coefficient of determination of the linear fit of the phase function is indicating the linearity of the phase retardation by the SLM.

$$\varphi(cv) = 2\,sin^{-1}\sqrt{P(cv)} \tag{1}$$

2.3. Characterization of intensity distribution, diffraction efficiency and result of material removal

To investigate the effects of the SLM-specific phase function and the benefits of the calibration on microstructuring computer generated holograms are applied at the SLM to shape the Gaussian laser beam into a quadratic top-hat profile. The calculation of the phase hologram was realized by the established Gerchberg-Saxton algorithm (GSA) [Gerchberg et al. (1972)]. In this iterative algorithm the amplitude in the diffraction plane P1 (Fig. 2) is assumed as an ideal Gaussian shaped beam and in the image plane P4 the desired amplitude is given by a top-hat.

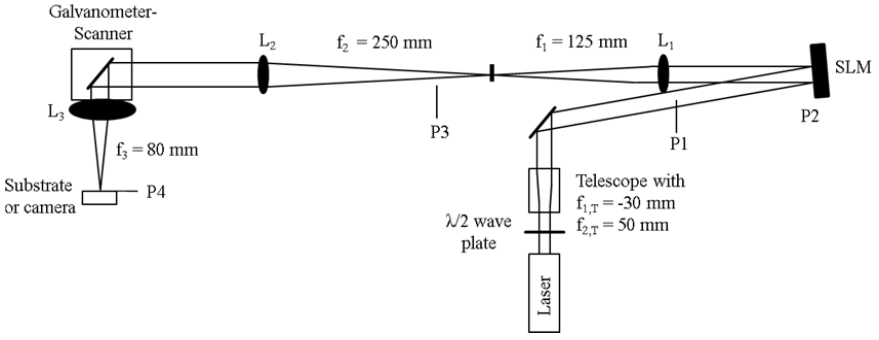

Fig. 2. Experimental setup for material processing, the evaluation of intensity profiles and the measurements of the diffraction efficiency.

Characterization of the top-hat is done according to DIN 13694 by camera-based (IDS UI-1220SE-M-GL R2) acquisition of the intensity in the image plane P4 [DIN EN ISO 13694:2014-03].The incident angle of the laser beam on the SLM with the diameter D_1 = 5.3 mm amounts to 4.9°. The shaped beam is collimated by a 6f-setup consisting of two convex lenses L1, L2 and the telecentric F-theta lens L3 with f_3 = 80 mm. To achieve the before mentioned advantages of cold material ablation a high homogeneity of the intensity represents the major goal. To evaluate the homogeneity the flatness factor *FLF* of the top-hat is assessed by the ratio of the mean intensity I_{mean} and the maximum intensity I_{max} of the top-hat (eq. (2)):

$$FLF(z) = {I_{mean}(z)}\Big/{I_{max}(z)} \tag{2}$$

The beam uniformity is evaluated by means of the speckle contrast *SC* of the top-hat plateau which represents the normalized standard deviation of the top-hat according to eq. (3) [Goodman (1976)].

$$SC(z) = {\sigma_I(z)}\Big/{I_{mean}(z)} \tag{3}$$

The diffraction efficiency η_{diff} of the first order, which allows for evaluation of the applied hologram and the SLM, is the quotient of the diffracted power P_1 and the power that is reflected at the SLM P_{refl}:

$$\eta_{diff} = {P_1}\Big/{P_{refl}} \tag{4}$$

Additionally, the total efficiency η_{tot} including the losses due to absorption at the liquid crystal layer and the reflective backplane is calculated according to eq. (5):

$$\eta_{tot} = {P_1}\Big/{P_{incident}} = {P_1}\Big/{(P_{refl} + P_{loss})} \tag{5}$$

The average laser power of the raw beam is measured before the SLM at P1 and of the non-diffracted as well as the diffracted parts are acquired after the SLM at P3 respectively P4. Additionally to these characterization methods, the steel alloy 1.2379 is processed with the shown setup. The generated microstructure is topographically characterized by means of laser scanning microscope (LSM) measurements. The ablation efficiency is calculated by the ratio of ablated volume depending on the applied pulse energy in the top-hat.

3. Results and discussion

3.1. Specifications of the investigated spatial light modulators

The specifications of the investigated SLMs are described in Tab. 1. The relevant data is selected from online provided specifications [Hamamatsu, BNS, Holoeye (2016)]. The resolution describes the number of pixels along the vertical and horizontal axis of the SLM. The pixel pitch characterizes the distance of the centers of adjacent pixels. This distance limits the maximum spatial frequency, and hence the maximum diffraction angle which can be achieved. The fill factor (*FF)* represents the coverage of the reflective coating by the pixelated surface. Due to the isolation for pixelization a separation gap is necessary, so that a density of 100 % of the reflective coating is not achievable. A common technique to overcome this issue is to fill up the separation gap before the reflective coating is deposited as it is applied for SLM **B**. The active area is a geometric measure of the pixelated size of the SLM. In the presented investigation, the operation wavelength of the considered systems is limited to either 532 nm or 1064 nm but the manufacturers provide systems for most wavelengths with adapted liquid layer thickness and a suitable reflective coating.

For laser material processing one will choose the system **B** because of its superior fill factor, which is often used as an indicator of the efficiency of the system. The SLM **C** is only available with a metallic reflection coating and thus is less suitable for laser material processing due to the inherently low damage threshold of this type of coating. In the following, we present additional data characterizing the optical response of the three tested systems, which are important to assess system's performance. Our measurements show that the provided specifications are not sufficient to properly describe the systems.

Table 1. Specifications of the investigated SLMs

Abbreviation in the text	**A**	**B**	**C**
SLM model	Hamamatsu – X11840	BNS	Holoeye – LETO
Resolution	800 x 600	512 x 512	1920 x 1080
Pixel pitch	20 µm	15 µm	6.4 µm
Fill factor	98%	100%	93%
Active area	16 x 12 mm	7.68 x 7.68 mm	12.5 x 7.1 mm
Phase levels for 2 π	256 (8 bit)	256 (8 bit)	256 (8 bit)
Operation wavelength	532 nm and 1064 nm	1064 nm	532 nm
Reflective coating	Dielectric	Dielectric	Metallic

3.2. SLM-specific phase function

Applying measurement method described in section 2.2, the phase function of the SLMs **A** and **B** is determined at 1064 nm wavelength, while system **C** is characterized at 532 nm. For each system a sinusoidal function of the power is clearly visible (Fig. 3a). While **B** shows no response for the first 60 control values (cv), the system **A** and **C** induce a change even in the first cv. Furthermore, the low standard deviation is an indicator for spatial uniformity of the phase function over the whole active area. The uniformity is represented by the mean standard deviation which is $S = 0.0505$ for system **C** and $S = 0.0597$ for SLM **A**. For the system **B** it is much higher with $S = 0.1075$.

The phase function is calculated according to equation (1) for all three SLMs as depicted in Fig. 3b). For each system, a linear fit is calculated whereby the coefficient of determination (R^2) is representing the linearity of the phase response of the system. Here, **A** shows the best linear behavior with a $R^2 = 0.9999$. **C** and **B** are determined to 0.9859 and 0.9042, respectively. From the low mean standard deviation and the high coefficient of determination the SLMs **A** and **C** can be operated with a linear phase function that can be globally applied for all pixels. In contrast to the individual phase function has to be considered for each section of SLM **B**. The apparent nonlinear behavior of the SLM **B** results in a corrected dynamic range of 164 phase levels. For the system **A** as it is capable to shift 2.57π the dynamic range amounts to 194 phase levels. The SLM **C** is measured with 256 phase levels for 2π. This is reasoned in a scaling operation performed within the driving circuits of the device.

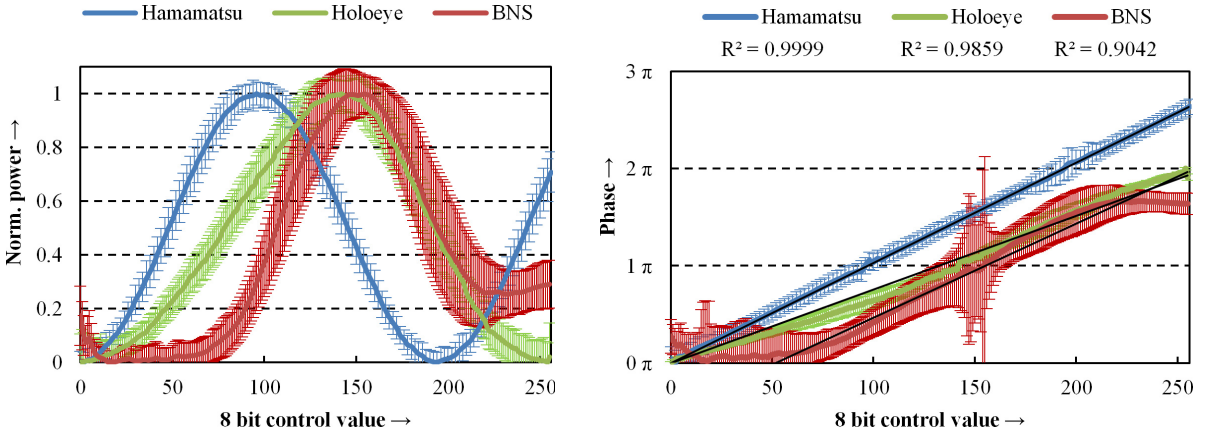

Fig. 3. (a) Power function and (b) phase function.

3.3. Effects of SLM-specific phase response on beam quality and diffraction efficiency

Based on the evaluation of the phase function of the different SLMs the system **B** has to be corrected to achieve the desired spatial uniform phase response. For the assessment of the effect of this correction the beam profile as well as the efficiency of three configurations are discussed:

(I) the non-compensated SLM **A**,
(II) the non-compensated SLM **B** and
(III) the compensated SLM **B**.

Compensation of each phase hologram is done as approved by *Engström et al.* The desired hologram is multiplied with a seventh order polynomial of the evaluated phase function as this order has shown comparatively low mean and low maximum phase error if 32 central SLM subregions are assessed. In optical trapping experiments, the polynomial correction method of the phase led to similar stiffness of parallel 5 traps which indicates the uniformity of distributed intensity [Engström et al. (2013)]. The phase holograms which are applied in configuration (I) to (III) are shown in Fig. 4. On the left side, the non-compensated 800 by 600 px hologram of configuration (I) and the 512 by 512 hologram of configuration (II) which transform the Gaussian raw beam into a 70 µm x 70 µm top-hat are depicted. On the right, the phase-mask of configuration (III) is shown.

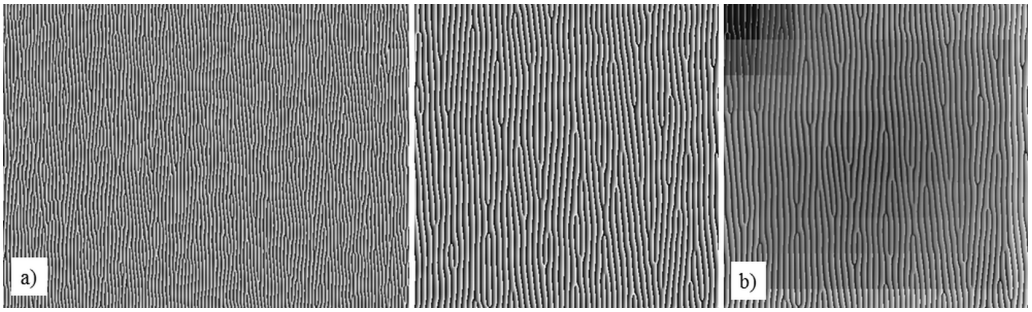

Fig. 4. (a) Holograms of configuration (I) respectively (II) and (b) corrected hologram of configuration (III) of a 70 µm square top-hat.

The measured intensity profile in the image plane P4 of lens L3 (Fig. 2) which is shaped by each of the three configurations is shown in Fig. 5. There are no significant speckles occurring in the acquired top-hat profile because this camera-based measured intensities show the result of the time averaging of subsequent holograms. According to *Amako et al.* a finite number of holograms which are calculated based on different initial phase distributions are applied and integrated to get one picture for evaluation [Amako et al. (1995)]. In this paper, 64 different phase holograms are applied.

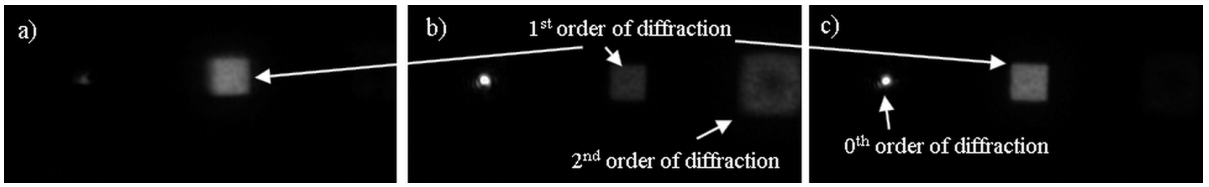

Fig. 5. Intensity in the image plane of lens L3 (a) in configuration (I) and (b) and (c) the SLM **B** in configuration (II) and (III), respectively.

There are no obvious differences for the shape and homogeneity of the top-hat in the first order in Fig. 5. However, the more detailed evaluation of the top-hat according to DIN 13694 shows that the top-hat transformed by SLM **A** has the highest flatness factor (Fig. 6a) which should be $FLF = 1$ in the case of an ideal top-hat. The flatness does not change significantly due to correction of the hologram at SLM **B**. Flatness factor of configuration (II) and (III) do not exceed the flatness achieved by configuration (I). The top-hat shaped by configuration (I) shows the best respectively lowest speckle contrast *SC*, too (Fig. 6a). Thereby, the correction of the phase response decreases the

speckle contrast. Both evaluated parameters show that the compensation does not lead to a higher beam quality than the top-hat shaped by SLM **A**. The effect of the observed comparatively low differences on the quality of generated microstructures is discussed later on in chapter 3.4.

The compensation mainly affects the diffraction efficiency as it can be qualitatively observed in Fig. 5, too. The correction of SLM **B** leads to a significantly higher diffraction efficiency (Fig. 6b). The non-diffracted zeroth order has a significantly lower grey value in configuration (I) than in configuration (III) and (II). Additionally, the intensity of the second order of diffraction is lower due to compensation, too. The diffraction efficiency of the SLM **A** measured at plane P4 is $\eta_{diff} = 67.9\ \%$ (Fig. 6b). Configuration (II) suffers from comparatively low diffraction efficiency of $\eta_{diff} = 15.7\ \%$. The calibration nearly quadruples the diffraction efficiency. Therefore, the diffraction efficiency of configuration (III) is still lower than configuration (I). Although the fill factor of SLM **B** $FF = 100\%$ is higher than the one of SLM **A** with $FF = 98\%$ the diffraction efficiency does not attain the one of SLM **A**. Therefore, it can be concluded that the diffraction efficiency is not only affected by the hardware specification, which the manufacturers provide. The necessary compensation of the phase response in the case of SLM **B** leads to more time-consuming hologram calculation. Thus, the compensation decreases the frame rate and is disadvantageous for beam shaping operations, which require high frame rates for hologram variation at the SLM for laser material processing.

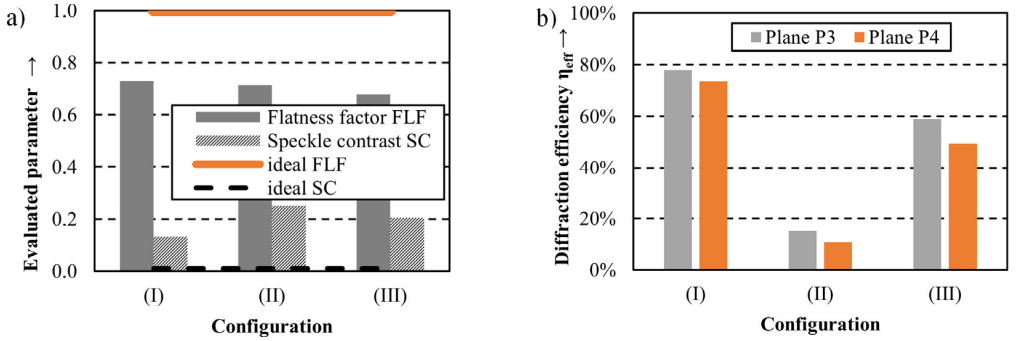

Fig. 6. (a) Flatness factor *FLF* and speckle contrast *SC* of the 70 x 70 µm top-hat as well as (b) diffraction efficiency η_{eff} of the first order of diffraction measured at plane P3 and P4 for the hologram to shape the top-hat.

3.4. Quality, ablation efficiency and total efficiency of material removal

Using the experimental setup in Fig. 2 the steel alloy 1.2379 is irradiated and processed with the 70 µm · 70 µm top-hat at different fluences. For material ablation $N = 640$ laser pulses were applied with 64 individually calculated holograms. Each hologram is applied for a sequence of ten laser pulses, so that asequence of the 64 holograms is shown once. The laser pulse frequency was chosen to $f_P = 10$ Hz which is lower than the switching frequencies of the investigated SLMs and enables hologram switching between subsequent laser pulses. The generated squared microstructures show neither any configuration-dependent significant difference of the dimensions nor of the shape of the structure contour (Fig. 7). The compensation of the phase error does not significantly improve the quality of the top-hat profile regarding the mean surface roughness *Sa* (Fig. 8a). The roughness of the bottom of the microstructures is characterized by fluence dependent occurring nano-ripples and microcones which stochastically arise in picosecond laser structuring due to interference effects at the initial surface roughness [Liu et al. (2013)]. Because of the small observed changes of the roughness as well as the flatness factor and the speckle contrast the computing assuming compensation is not justified from the of ablation quality, too. This marginal improvement of top-hat homogeneity would be beneficial or required for ablation processes which are very sensitive to intensity variations e.g. microstructure generation with very low roughness at the structure bottom. However, further methods of intensity optimization such as closed-loop control of the intensity profile probably would increase beam quality more drastically compared to the presented compensation.

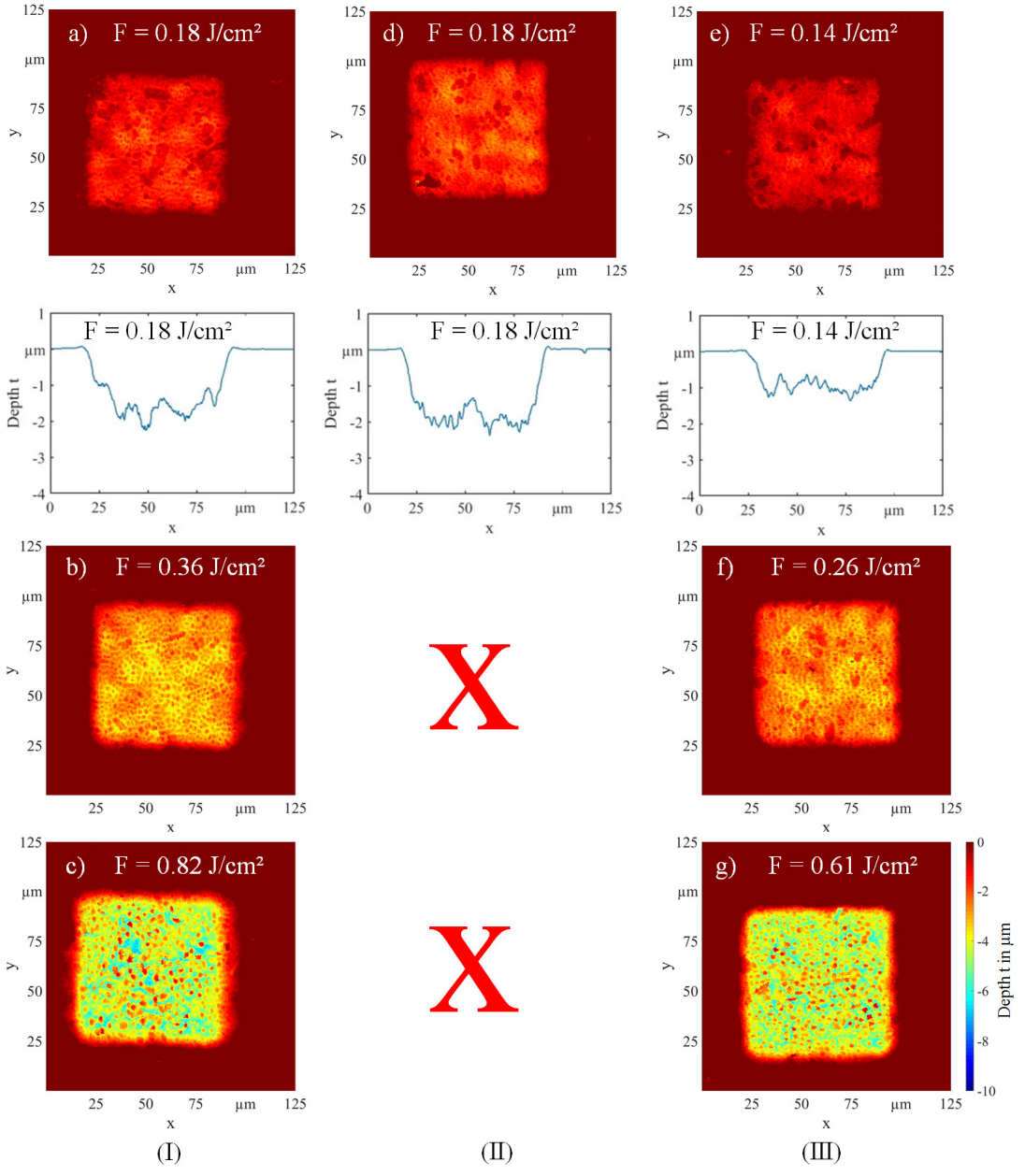

Fig. 7. Height and exemplary cross-section of the microstructure generated with (a)-(c) configuration (I) (SLM **A**), (d) configuration (II) (non-compensated SLM **B**) and (f)-(h) configuration (III) (compensated SLM **B**) at different fluences F (64 holograms, f_P = 10 Hz, N = 640).

The major effect of phase error compensation is observed for the significant increase of the diffraction efficiency η_{diff}. The higher diffraction efficiency leads to a higher pulse energy E_P which is available for material ablation. As the maximum ablation efficiency of picosecond laser based removal for steel alloys can be observed in a fluence range of F = 0.2 J/cm² to 0.3 J/cm² (Fig. 8b) which coincides well with investigations of further studies from Neuenschwander et al. (2013) the diffraction efficiency is very important to realize efficient microstructuring processes. Without the compensation of the spatially dependent phase error the optimal fluence for maximum

ablation efficiency cannot be achieved (Fig. 8b). This limit of the pulse energy which can be irradiated on the SLM results in the fact, that the same fluences which were applied by configuration (I) and (III) even cannot be realized by configuration (II) (Fig. 7).

Thus, different diffraction efficiencies lead to high differences of the total efficiency of SLM beam shaping systems applied for USP laser based material removal (Fig. 8c). The lowest total efficiency of configuration (II) can be significantly increased by phase error compensation of configuration (III). However, the highest total efficiency of configuration (I) is still not reached although the diffraction efficiencies of configuration (I) and (III) do not differ by a factor of 2 as the total efficiency does. This strong discrepancy of the total performance of both SLMs is mainly caused by losses due to absorption at the SLM display which amounts to 4.2 % for SLM **A** and 16.6 % for SLM **B** at the applied laser pulse frequency f_P = 10 Hz.

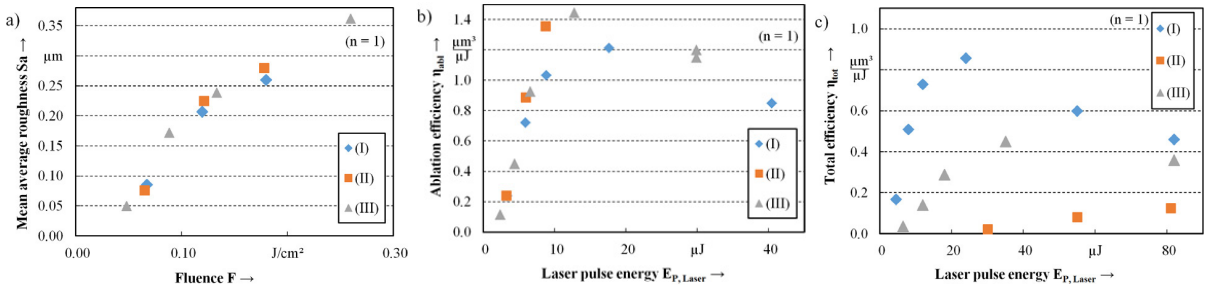

Fig. 8. Configuration dependent (a) mean average roughness *Sa* of the bottom of the microstructures, (b) ablation efficiency η_{abl} and (c) total efficiency η_{tot} of material removal applying SLM-based beam shaping (64 holograms, f_P = 10 Hz, N = 640).

Thus, effective reflectivity and diffraction efficiency predominantly affect the performance of LCoS based SLMs and still limit the possible processing speed in USP laser based structuring with holographic beam shaping. The absorption of too high pulse energies would lead to the irreversible damage of the reflective backplane of the LCoS while the linear absorption of high laser powers can change the phase response due to LCoS heating especially at pulse frequencies in the kilohertz range [Beck (2010)].

4. Conclusion

In our investigations we evaluated the capability of three SLM systems from different manufacturers regarding laser microstructuring with ultrashort-pulsed lasers (USP). As the data provided by the manufacturers may not be sufficient to precisely adjust the phase response of the SLM the spatially dependent phase function was determined experimentally. The systems from Hamamatsu and Holoeye show high linearity and good agreement with the provided data. The tested SLM from BNS has shown a nonlinear behavior with large spatial variations making a sophisticated compensation reasonable.

The lack of a dielectric coating with a high damage threshold of the Holoeye SLM made this system inappropriate for applications utilizing high pulse energies. The remaining two SLMs, one with an excellent linear and the second one with a nonlinear phase response, are tested for laser microprocessing. The compensation of the spatial phase deviation of the SLM does not show significant improvement of the beam quality as well as the ablated microstructure but quadruples the diffraction efficiency of top-hat beam shaping as well as the total efficiency of the ablation process.

Acknowledgements

The authors gratefully acknowledge funding of the project “Lubrication free forming with tailored tribological conditions” within the DFG priority programme 1676 “Dry metal forming - sustainable production through dry

processing in metal forming" and the funding of the Erlangen Graduate School in Advanced Optical Technologies (SAOT) by the German National Science Foundation (DFG) in the framework of the excellence initiative.

References

Amako, J., Miura, H., Sonehara, T., 1995. Speckle-noise reduction on kinoform reconstruction using a phase-only spatial light modulator, Applied Optics 34(17), 3165-3171.

Beck, R., 2010. Adaptive Optics for Laser Processing, Heriot-Watt-University, Edinburgh.

Bischoff, C., Jäger, E., Umhofer, U., 2015. Beam shaping optics for process acceleration – Increasing the productivity of laser micromachining. Laser Technik Journal 3, 53-57.

BNS, 2016. http://bnonlinear.com/pdf/XYSeriesDS0909.pdf.

Chichkov, B.N, Momma, C., Nolte, S., von Alvensleben, F., Tünnermann, A., 1996. Femtosecond, picosecond and nanosecond laser ablation of solids, Applied Physics A, 109-115.

Deutsches Institut für Normung, Optik und Photonik - Laser und Laseranlagen, 2014. Prüfverfahren für die Leistungs-(Energie-)dichteverteilung von Laserstrahlen. DIN EN ISO 13694:2014-03, Beuth, Berlin.

Donnet, C., Erdemir, A., 2008. Tribology of Diamond-like Carbon Films, Springer US, 571-590.

Engström, D., Persson, M., Bengtsson, J., Goksör, M., 2013. Calibration of spatial light modulators suffering from spatial varying phase response, Optics Express 21(13), 16086-16103.

Gecys, P., Raciukaitis, G., Miltenis, E., Braun, A., Ragnow, S., 2011. Scribing of Thin-film Solar Cells with Picosecond Laser Pulses, Physics Procedia 12, 141-148.

Gerchberg, R.W., Saxton, W.O., 1972. A practical algorithm for the determination of the phase from image and diffraction plane pictures, Optik 35, 237.

Goodman, J.W., 1976. Some fundamental properties of speckle, Journal of the Optical Society of America 66, 1145-1150.

Häfner, T., Reg, Y., Hetzner, H., Schmidt, M., 2013. Microstructuring Tools for Sheet Bulk Metal Forming - A Designated Application for Picosecond Laser, Journal of Laser Micro/Nanoengineering 8(1), 39-44.

Hamamatsu, 2016. http://www.hamamatsu.com/resources/pdf/ssd/x10468_series_etc_kacc1172e.pdf.

Holoeye, 2016. http://holoeye.com/wp-content/uploads/LETO_Phase_Only_Modulator.pdf.

Liu, B., Wang, W., Jiang, G., Mei, X., Wang, K., Wang, J., 2013. Formation of Porous Structure with Subspot Size under the Irradiation of Picosecond Laser Pulses, Journal of Nanomaterials 2013, 1-9.

Neuenschwander, B., Jäggi, B., Schmid, M., 2013. Möglichkeiten und Grenzen neuer Lasersysteme für die Fertigungstechnik in der Mikrobearbeitung. Tagungsband LEF 2013, 54-73.

Rung, S., Bischoff, C., Jäger, E., Umhofer, U., Hellmann, R., 2014. Laser Thin Film Ablation with Multiple Beams and Tailored Beam Profiles, Proceedings of SPIE 8967, Laser Applications in Microelectronic and Optoelectronic Manufacturing (LAMOM) XIX, 89670.